International Journal of Minerals, Metallurgy and Materials
Volume 27, Number 6, June 2020, Page 830
https://doi.org/10.1007/s12613-019-1923-5

Design of $(GO/TiO_2)_N$ one-dimensional photonic crystal photocatalysts with improved photocatalytic activity for tetracycline degradation

Huan-huan Wang[1),*], *Wen-xiu Liu*[2),*], *Jing Ma*[1)], *Qian Liang*[1)], *Wen Qin*[1)], *Patrick Osei Lartey*[1)], *and Xiao-jiang Feng*[2)]

1) Institute of New Carbon Materials, Taiyuan University of Technology, Taiyuan 030024, China
2) Zhongguancun Institute of Human Settlements Engineering and Materials, Beijing 100083, China
(Received: 21 June 2019; revised: 10 October 2019; accepted: 16 October 2019)

Abstract: $(GO/TiO_2)_N$ (GO represents graphene oxide, and *N* represents the period number of alternate superposition of two dielectrics) one-dimensional photonic crystal with different lattice constants was prepared via the sol–gel technique, and its transmission characteristics for photocatalysis were tested. The results show that the lattice constant, filling ratio, number of periodic layers, and incident angle had effects on the band gap. When the lattice constant, filling ratio, number of periodic layers, and incident angle were set to 125 nm, 0.45, 21, and 0°, respectively, a gap width of 53 nm appeared at the central wavelength (322 nm). The absorption peak of the photocatalyst at 357 nm overlapped the blue edge of the photonic band gap. A slow photon effect region above 96% reflectivity appeared. The degradation rate of tetracycline in $(GO/TiO_2)_N$ photonic crystal was enhanced to 64% within 60 min. Meanwhile, the degradation efficiency of $(GO/TiO_2)_N$ one-dimensional photonic crystal was effectively improved compared with those of the GO/TiO_2 composite film and GO/TiO_2 powder.

Keywords: one-dimensional photonic crystal; translight software; transmission characteristics; photocatalytic performance; slow photon effect

1. Introduction

As an important oxide semiconductor material, titanium dioxide (TiO_2) features a high dielectric constant, refractive index, wide band gap, and especially good photocatalytic properties. It has been widely used in sensors, solar energy utilization, the catalytic industry, and environmental control [1–2]. Titanium oxide can absorb short-wave ultraviolet radiation due to its wide band gap (about 3.2 eV). Under illumination, electrons and holes that have an important influence on the photocatalytic effect are produced in TiO_2. However, the electrons and holes easily recombine during the transfer process, which greatly limits the TiO_2 photocatalytic effect [3–4].

As a two-dimensional carbon nanomaterial, graphene oxide (GO) exhibits the properties of hydrophilicity, electronegativity, easy modification, good biocompatibility, high mechanical strength, and large specific surface area [5]. Vallejo *et al*. [6] indicated that the removal rate of methyl blue (MB) with the degradation of GO–TiO_2 thin films reached 33% within 100 min under visible light irradiation. Qi *et al*. [7] indicated that the photocatalytic degradation efficiency of rhodamine B (RhB) by modified nanosized metallic Ag particles modified graphene oxide–TiO_2 mesocrystals (Ag/GO–TMCs) was the highest after the irradiation of visible light for 3 h. That is, the combination of GO and TiO_2 would be beneficial to improve the photocatalytic efficiency of TiO_2.

In recent years, many studies have shown that the photocatalytic performance of semiconductor materials was significantly improved by introducing a photonic crystal structure, which is a kind of artificial optical material and its dielectric constant changes periodically [8–9]. A photonic crystal was first proposed by Yablonovitch [10] and John [11] in 1987. It was mainly used in photonic crystal polarizers and various optical devices such as nonlinear optical limiters, photonic band-edge lasers, and photonic fibers [12]. Photonic crystals are characterized by photonic band gap and photon localization [13–14]. The light-capture ability of photocatalytic materials is improved by the slow photon effect, which is a phenomenon describing the propagation of light at a lower group velocity near the edge of a photonic band gap.

*These authors contributed equally to this work.
Corresponding author: Jing Ma E-mails: majing@tyut.edu.cn; jingma1984@gmail.com

The absorbance of the photocatalyst increased due to the overlapping range of the slow photon and target spectrum [15–16]. Li *et al*. [17] have shown that the high specific surface area of nc-TiO_2/SiO_2 antipodal films can improve their optical absorption properties. When the absorption edge of TiO_2 coincides with the photonic band gap, the photocatalytic efficiency of liquid MB and solid rhodamine is significantly increased. However, a one-dimensional photonic crystal can achieve the same effect. Lu *et al*. [18] indicated that a C–Si one-dimensional photonic crystal solar cell with 12-μm active layer thickness could achieve a high photoelectric density of 32.6 $mA \cdot cm^{-2}$.

In the past decade, the potential environmental risks of antibiotics such as tetracycline attracted worldwide attention. Tetracycline in water can lead to water pollution [19–20]. In recent years, photocatalysis has attracted wide attention in various aspects of environmental pollution control [21–23].

In this work, to further improve the photocatalytic efficiency, $(GO/TiO_2)_N$ one-dimensional photonic crystal was prepared by the sol–gel method and spin coating. The precursor solution was prepared via the sol–gel method, and the films were prepared by spin coating. Slow photon effects were introduced into one-dimensional photonic crystals. The utilization and capture efficiency of incident photons were enhanced by the slow photon energy at the blue edge. The slow photon effect is utilized at the maximum absorption wavelength (357 nm) of tetracycline. The prepared photonic crystal showed the advantages of low dosage and easy recovery.

2. Calculation and experiment

2.1. Theoretical model

One-dimensional photonic crystals are extensively explored because of their simple structure and easy fabrication, as well as their omnidirectional energy gap structures, which are similar to those of two-dimensional and three-dimensional photonic crystals. The transfer matrix method [24], plane wave expansion method [25], finite-difference time domain method, and Green's function method [26] are used to study the photonic crystal band gap. The transfer matrix method is simple and features easy calculation. Maxwell's equations are used to solve the electric and magnetic fields on two adjacent layers, and the transfer matrix is acquired. Fig. 1 shows the structure of $(GO/TiO_2)_N$ (N is the period number of alternate superposition of two dielectrics) one-dimensional photonic crystal. The incident angle is θ. The black part represents GO, with refractive index $n_{GO} = 2$ [27], and the white part represents TiO_2, with refractive index $n_{TiO_2} = 3$ [28]. GO and TiO_2 are arranged alternately to form multilayers. The structure is periodically arranged in the z direction and extends infinitely in the x and y directions, where d_{GO} and d_{TiO_2} are the thicknesses of GO and TiO_2 dielectric layers, respectively, and one periodic thickness is $d = d_{GO} + d_{TiO_2}$. If the electromagnetic field at the interface between adjacent dielectric layers meets the boundary conditions, the interaction between each dielectric layer and the light wave can be represented by the characteristic matrix $\boldsymbol{M}_j$, then for the field vectors $\boldsymbol{E}_{\mathrm{I}}$, $\boldsymbol{H}_{\mathrm{I}}$, $\boldsymbol{E}_{\mathrm{II}}$, and $\boldsymbol{H}_{\mathrm{II}}$ on both sides of the j layer (Fig. 2) can be connected by the characteristic matrix [29], as shown in Eq.(1).

$$\begin{bmatrix} \boldsymbol{E}_{\mathrm{I}} \\ \boldsymbol{H}_{\mathrm{I}} \end{bmatrix} = \boldsymbol{M}_j \begin{bmatrix} \boldsymbol{E}_{\mathrm{II}} \\ \boldsymbol{H}_{\mathrm{II}} \end{bmatrix} \tag{1}$$

where I and II represent the upper and lower interfaces of the j layer, $\boldsymbol{E}_{\mathrm{I}}$, $\boldsymbol{H}_{\mathrm{I}}$, $\boldsymbol{E}_{\mathrm{II}}$, and $\boldsymbol{H}_{\mathrm{II}}$ represent the electric field $\boldsymbol{E}$ and the magnetic field $\boldsymbol{H}$ at the two interfaces I and II.

Fig. 2 shows the propagation of light in the j-layer dielectric of one-dimensional photonic crystal in a transverse electric mode (TE mode). In the Fig. 2, n_j is the refractive index

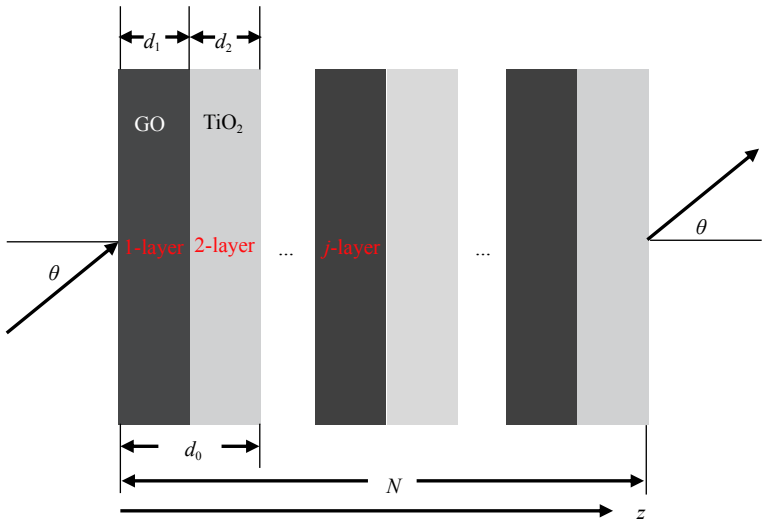

Fig. 1. Schematic diagram of $(GO/TiO_2)_N$ one-dimensional photonic crystal structure.

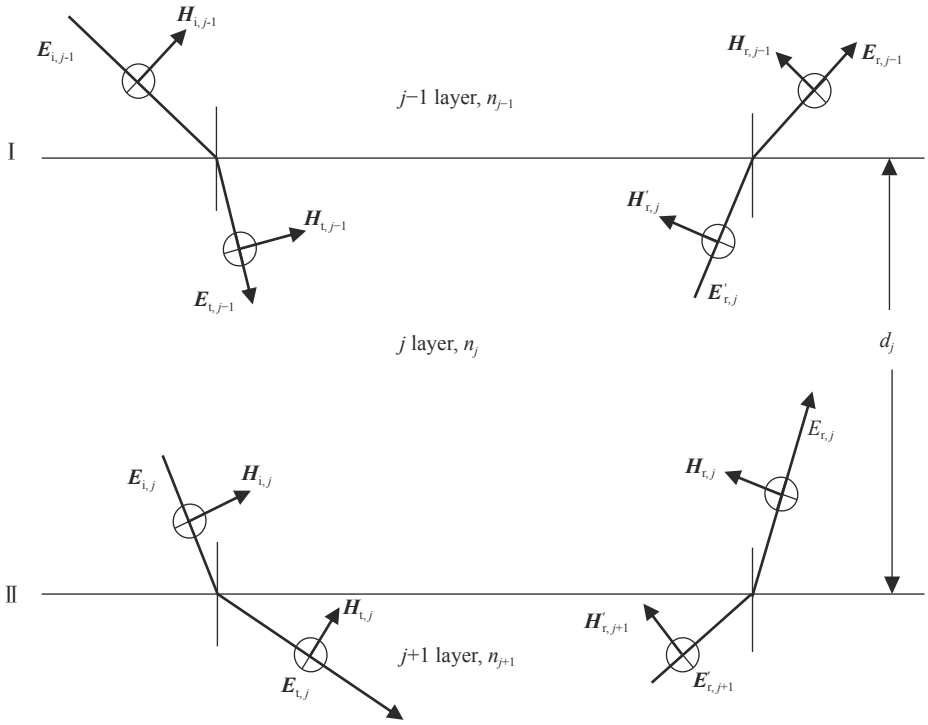

Fig. 2. Propagation of light in the *j*-layer dielectric of one-dimensional photonic crystal.

of the j layer, and n_{j-1} and n_{j+1} are the refractive index of the adjacent dielectric layer. On the interface I possess the incident light wave $\boldsymbol{E}_{\mathrm{i},j-1}$, the reflected light wave $\boldsymbol{E}_{\mathrm{r},j-1}$, the transmitted light wave $\boldsymbol{E}_{\mathrm{t},j-1}$, and the light wave $\boldsymbol{E}'_{\mathrm{r},j}$ incident on the interface I from the dielectric of j layer; the corresponding magnetic fields on the interface I are $\boldsymbol{H}_{\mathrm{i},j-1}$, $\boldsymbol{H}_{\mathrm{r},j-1}$, $\boldsymbol{H}_{\mathrm{t},j-1}$, $\boldsymbol{H}'_{\mathrm{r},j}$, respectively. On the interface II possess the incident light wave $\boldsymbol{E}_{\mathrm{i},j}$, the reflected light wave $\boldsymbol{E}_{\mathrm{r},j}$, the transmitted light wave $\boldsymbol{E}_{\mathrm{t},j}$, and the light wave $\boldsymbol{E}'_{\mathrm{r},j+1}$ incident on the interface II from the dielectric of j+1 layer; the corresponding magnetic fields on the interface II are $\boldsymbol{H}_{\mathrm{i},j}$, $\boldsymbol{H}_{\mathrm{r},j}$, $\boldsymbol{H}_{\mathrm{t},j}$, $\boldsymbol{H}'_{\mathrm{r},j+1}$, respectively.

When the free charge density or current density in the dielectric is 0, the tangential components of the electric field $\boldsymbol{E}$ and the magnetic field $\boldsymbol{H}$ at the two interfaces I and II are continuous. Therefore, the field vectors $\boldsymbol{E}_{\mathrm{I}}$, $\boldsymbol{H}_{\mathrm{I}}$, $\boldsymbol{E}_{\mathrm{II}}$, and $\boldsymbol{H}_{\mathrm{II}}$ can be calculated by Eqs. (2)–(3).

$$\begin{cases} \boldsymbol{E}_{\mathrm{I}} = \boldsymbol{E}_{\mathrm{i},j-1} + \boldsymbol{E}_{\mathrm{r},j-1} = \boldsymbol{E}_{\mathrm{t},j-1} + \boldsymbol{E}'_{\mathrm{r},j} \\ \boldsymbol{H}_{\mathrm{I}} = \boldsymbol{H}_{\mathrm{i},j-1}\cos\theta_{\mathrm{i},j-1} - \boldsymbol{H}_{\mathrm{r},j-1}\cos\theta_{\mathrm{i},j-1} = \\ \quad \boldsymbol{H}_{\mathrm{t},j-1}\cos\theta_{\mathrm{i},j} - \boldsymbol{H}'_{\mathrm{r},j}\cos\theta_{\mathrm{i},j} \end{cases} \tag{2}$$

$$\begin{cases} \boldsymbol{E}_{\mathrm{II}} = \boldsymbol{E}_{\mathrm{i},j} + \boldsymbol{E}_{\mathrm{r},j} = \boldsymbol{E}_{\mathrm{t},j} + \boldsymbol{E}'_{\mathrm{r},j+1} \\ \boldsymbol{H}_{\mathrm{II}} = \boldsymbol{H}_{\mathrm{i},j}\cos\theta_{\mathrm{i},j} - \boldsymbol{H}_{\mathrm{r},j}\cos\theta_{\mathrm{i},j} = \\ \quad \boldsymbol{H}_{\mathrm{t},j}\cos\theta_{\mathrm{i},j+1} - \boldsymbol{H}'_{\mathrm{r},j+1}\cos\theta_{\mathrm{i},j+1} \end{cases} \tag{3}$$

When the electromagnetic field propagates, it will produce a different phase φ. From this, the single-layer transmission matrix $\boldsymbol{M}_{\mathrm{j}}$ can be deduced as follows:

$$\boldsymbol{M}_j = \begin{bmatrix} \cos\varphi_j & \mathrm{i}\times\sin\varphi_j/\eta_j \\ \mathrm{i}\times\eta_j\times\sin\varphi_j & \cos\varphi_j \end{bmatrix} \tag{4}$$

$$\varphi_j = -\frac{2\pi}{\lambda} n_j d_j \cos\theta_j \tag{5}$$

$$\eta_j = \sqrt{\frac{\varepsilon_0}{\mu_0}} n_j \cos\theta_j \tag{6}$$

where d_j is the geometric thickness of the j-layer, $\mathrm{i} = \sqrt{-1}$ corresponding to lossless in dielectric layer, ε_0 is the dielectric constant in the vacuum, μ_0 is the permeability in the vacuum, and λ is the central wavelength of the band gap, and η_j is the optical admittance values of n_j. That is, the transfer matrix of one-dimensional photonic crystal with a periodic structure can be written as follows:

$$\begin{bmatrix} \boldsymbol{E}_{\mathrm{I}} \\ \boldsymbol{H}_{\mathrm{I}} \end{bmatrix} = (\boldsymbol{M}_1\boldsymbol{M}_2\cdots\boldsymbol{M}_N)\begin{bmatrix} \boldsymbol{E}_{(N+1)} \\ \boldsymbol{H}_{(N+1)} \end{bmatrix} = \boldsymbol{M}\begin{bmatrix} \boldsymbol{E}_{(N+1)} \\ \boldsymbol{H}_{(N+1)} \end{bmatrix} \tag{7}$$

$$\boldsymbol{M} = \boldsymbol{M}_1\boldsymbol{M}_2\cdots\boldsymbol{M}_N = \begin{bmatrix} A & B \\ C & D \end{bmatrix} \tag{8}$$

According to Eq. (8), the electromagnetic field equation at the interface of the first layer and the N+1 layer can be written, and the total reflection coefficient r and the total transmission coefficient t of the photonic crystal can be obtained.

$$r = \frac{A\eta_0 + B\eta_0^2 - C - D\eta_0}{A\eta_0 + B\eta_0^2 + C + D\eta_0} \tag{9}$$

$$t = \frac{2\eta_0}{A\eta_0 + B\eta_0^2 + C + D\eta_0} \tag{10}$$

$$\eta_0 = \sqrt{\frac{\varepsilon_0}{\mu_0}}\cos\theta \tag{11}$$

where η_0 is the effective optical admittance, and μ_0 is the permeability in the vacuum.

Therefore, the reflectivity R and transmissivity T of one-dimensional photonic crystals are as follows:

$$R = r^2 \tag{12}$$

$$T = t^2 \tag{13}$$

The central wavelength and gap width of the band gap are affected by the lattice constant, filling ratio, number of periodic layers, and incident angle [30]. In one-dimensional photonic crystals, the lattice constant refers to the thickness of a composite layer of GO and TiO_2.

The band gap characteristics of photonic crystals include central wavelength and gap width, which are mainly related to the lattice constant, filling ratio, number of periodic layers, and incident angle. In this paper, Translight software (COPYRIGHT A. L. Reynolds 2000) was used to carry out the main numerical simulation calculation. The range of structural parameters of the $(GO/TiO_2)_N$ one-dimensional photonic crystals designed in this study was determined by the following steps [31]: the lattice constant d could be determined by $n_{GO}d_{GO} = n_{TiO_2}d_{TiO_2} = \lambda/4$; here, the refractive indexs of $n_{TiO_2} = 3$ and $n_{GO} = 2$ were adopted.

2.2. Experimental

Butyl titanate was purchased from Tianjin Damao Chemical Reagent Factory; glacial acetic acid from Tianjin Beichen Fangzheng Reagent Factory; GO from Shanghai Carbon Source Huigu New Material Technology Co., Ltd.; acetone, anhydrous ethanol, and slide from Tianjin Zhiyuan Chemical Reagent Co., Ltd.; deionized water was made in the laboratory.

Titanium dioxide sol was prepared according to the literature [22]. The solution after reaction was placed in a dryer for use. The GO concentration was 6 mg/mL. 50 mg of GO was weighed with an electronic balance, and the corresponding deionized water was measured. The two materials were mixed in a 25 mL beaker and then ultrasonicated. When the temperature of the solution became too high, the ultrasonic wave stopped and continued after the solution cooled. The cumulative ultrasonic time was not less than three hours. After that, an ultrasonic cleaner was used to continue the ultrasound for more than 12 h, and the reaction solution was placed in the dryer for use.

The slide was first cleaned with acetone, and then with deionized water, and finally with ethanol. The as-prepared TiO_2 sol was diluted twice with absolute ethanol. Then, GO solution and TiO_2 sol were alternately spin-coated on the slide. Afterward, each spin-coated layer was placed in an oven at 40°C for 10 min.

2.3. Photocatalytic experiments

In the self-made photocatalytic reaction chamber, tetracycline (TC) was added as the substrate of simulated dye wastewater, and the decolorization rate of tetracycline solution was applied to investigate the photocatalytic degradation performance. The light source was a xenon lamp. The system was cooled by circulating water. Afterward, 0.5 mg of tetracycline was added to 100 mL of deionized water, and then, the prepared photocatalyst samples were added to the deionized water. The photodegradation experiment began 20 min after stirring in the dark. Every 10 min, 5 mL of suspension was extracted from the photocatalytic system. Continuous magnetic stirring was used to carry out photodegradation experiments, and the photodegradation reaction lasted 120 min. The samples were separated by a centrifuge. The ratio of absorption of different time (C) to that of 0 min (C_0) was used to evaluate the concentration changes of TC. The absorbance A of the supernatant was determined (the maximum absorption wavelength of tetracycline solution was 357 nm). Relative absorbance was used to represent the relative concentration of the solution.

3. Results and discussion

3.1. Effect of lattice constant on photonic band gap

The gap width and central wavelength of $(GO/TiO_2)_N$ one-dimensional photonic crystal investigated in this study varied with the lattice constant, as shown in Fig. 3. The simulation conditions for transmission curve shown in the Fig. 3(a) were as follows: number of periodic layers $N = 21$, lattice constant $d = 125$ nm, filling ratio $d_{GO}/d = 0.45$, and incidence angle $\theta = 0°$. Fig. 3(a) shows that a photonic forbidden band with a width of 38 nm exists at the central wavelength 320 nm and a photonic forbidden band with a width of 155 nm exists at the central wavelength 650.5 nm. Figs. 3(b)–3(c) indicate that the incident light was inclined vertically and the gap width varied with the lattice constant when the filling ratio ($d_{GO}/d = 0.45$) and the number of periodic layers ($N = 21$) were constant. As seen in Figs. 3(b)–3(c), when the lattice constant d increased, the band gap became wider and gradually red-shifted to the long wave direction. While the lattice constant increased from 73 to 150 nm, the central wavelength shifted from 186.5 to 376 nm. Fig. 3(c) shows that the central wavelength of the band gap shifted from 380 to 765 nm, and the gap width increased from 90 to 190 nm. Compared with Fig. 3(b), Fig. 3(c) has a larger central wavelength and a wider photonic band gap.

3.2. Effect of filling ratio on photonic band gap

The band gap width and central wavelength of $(GO/TiO_2)_N$ one-dimensional photonic crystal investigated in

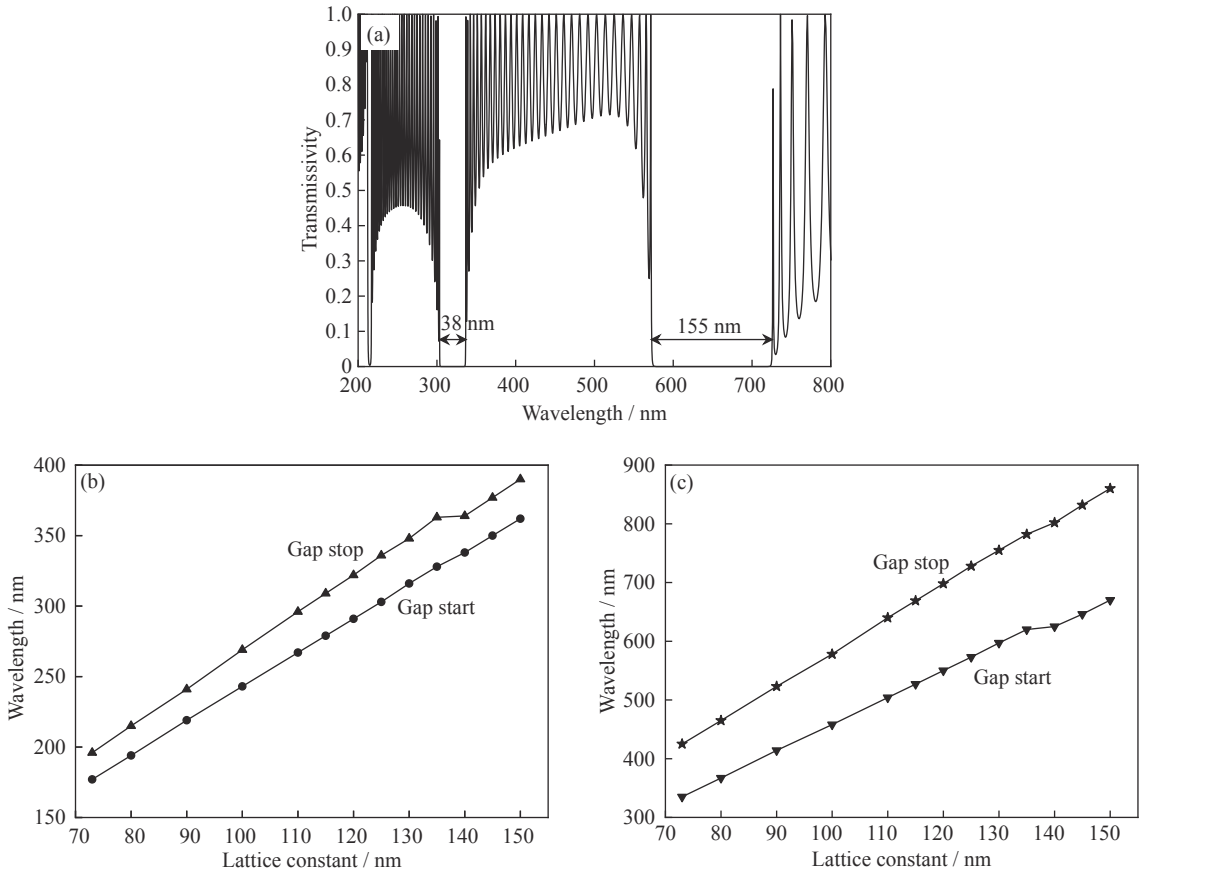

Fig. 3. Band gap curves of different lattice constants for $(GO/TiO_2)_N$ one-dimensional photonic crystal: (a) simulated transmission curve; (b) band gap width at low wavelength; (c) band gap width at high wavelength.

this study varied with the filling ratio, as shown in Fig. 4. When incident light was vertical, the simulation conditions were as follows: number of periodic layers $N = 21$ and lattice constant $d = 125$ nm. With the above parameters unchanged, the value of the filling ratio d_{GO}/d continuously increased. When the filling ratio $d_{GO}/d < 0.45$, the band gap gradually blue-shifted. The central wavelength gradually shifted from 752 to 650.5 nm and the gap width from 38 to 155 nm. When the filling ratio $d_{GO}/d > 0.45$, the band gap blue-shifted and the gap width decreased. The band gap center wavelength moved from 650.5 to 576 nm, and the gap width decreased from 155 to 34 nm.

3.3. Effect of periodic number on photonic band gap

Fig. 5 shows the transmission curve of the $(GO/TiO_2)_N$ one-dimensional photonic crystal structure under TE mode. It

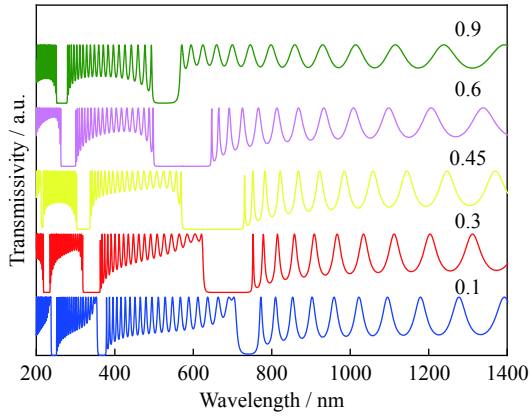

Fig. 4. Simulated transmission curves for different filling ratio of $(GO/TiO_2)_N$ one-dimensional photonic crystal.

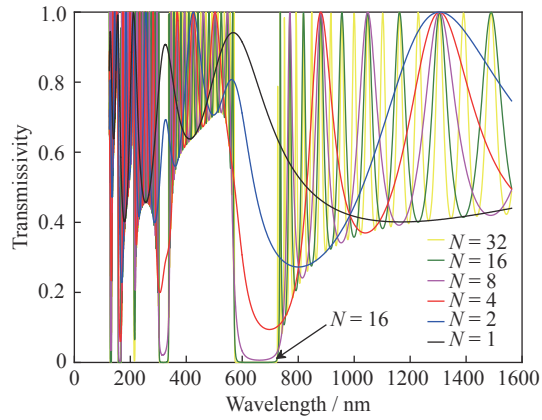

Fig. 5. Simulated transmission curves of different periodic layers of $(GO/TiO_2)_N$ one-dimensional photonic crystal.

can be observed from the Fig. 5 that a photonic band gap width of 155 nm exists at the central wavelength of 650.5 nm. When the number of periodic layers increased, the photonic band gap gradually tended to be stable, and the transmittance in the corresponding wavelength of 573–728 nm decreased. The photonic band gaps of the multilayers almost coincided when the number of periodic layers N was more than 16, and the transmittance reached 0 at the central wavelengths of 320 and 650.5 nm.

3.4. Effect of incident angle on band gap

To examine the effect of incident angle on the central wavelength and gap width, the variation diagrams of band gap from 0° to 90° were obtained by calculations. The external magnetic field is perpendicular to the wave vector, when the lattice constant (d = 125 nm), filling ratio (d_{GO}/d = 0.45), and number of periodic layers (N = 21) were constant, the band gap position and gap width of $(GO/TiO_2)_N$ one-dimensional photonic crystal varied with the incident angle. Fig. 6 shows the following: (1) when the incident angle equaled 0°, two band gaps of 38 and 190 nm were at the central wavelengths of 320 and 765 nm, respectively, and the gap width was the largest; (2) with the increase of the incident angle, the position of the central wavelength of the gap width moved to the short-wave direction, with the increase of the incident angle from 0° to 90°, the position of the central wavelength gradually moved from 650 to 598 nm; (3) with the increase of the incident angle, the gap width became narrower, the gap width was 144 nm at 0°, 128 nm at 30°, and 84 nm at 60°. That is, gap width decreased with the increase of incident angle. This shows that the incident angle affected the central wavelength and the gap width, and the gap width reached the maximum when the incident angle θ was 0°.

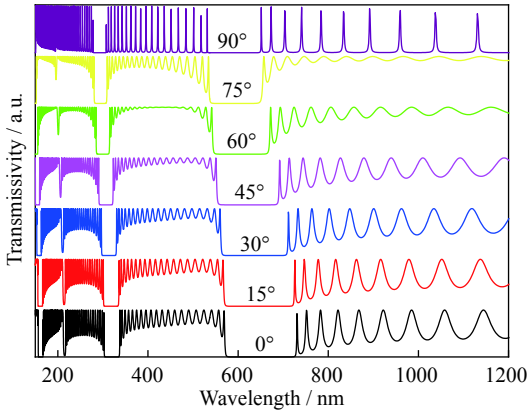

Fig. 6. Simulated transmission curves for different incident angles of $(GO/TiO_2)_N$ one-dimensional photonic crystal.

3.5. Transmittance curves of $(GO/TiO_2)_N$ one-dimensional photonic crystal

To verify the calculated central wavelength and gap width, the transmission properties of $(GO/TiO_2)_N$ one-dimensional photonic crystal were measured by an ultraviolet-visible spectrophotometer. The thicknesses of three films were measured by a stylus surface profiler. The transmission curves at different lattice constants, d = 73, 109, and 125 nm, were measured under a certain filling ratio (d_{GO}/d = 0.45), number of periodic layers (N = 21), and vertical incidence.

Fig. 7(a) presents a theoretical transmission curve with lattice constant d = 73 nm. Fig. 7(a) shows that a photonic band gap with a width of 100 nm exists at the central wavelength 370 nm. The experimental transmission curve (Fig. 7(b)) shows that a photonic band gap exists near the central wavelength 320 nm. The calculated transmission curve of $(GO/TiO_2)_N$ one-dimensional photonic crystal with lattice constant 109 nm is shown in Fig. 7(c). Fig. 7(c) shows that two band gaps exist at the central wavelength of 281.5 and 572 nm, while only one band gap appears at 276 nm in Fig. 7(d); this may due to the uneven composition of the films during spin coating. Fig. 7(e) shows the calculated transmission curve of $(GO/TiO_2)_N$ one-dimensional photonic crystal with a lattice constant of 125 nm. There are two band gaps at the central wavelengths of 320 and 650.5 nm. Fig. 7(f) shows that only one band gap with a gap width of 53 nm appears at 322 nm. There is an uncertainty of the width of the photonic band gap and of both the upper and lower limits of this gap. These uncertainties increase by increasing the tolerances of the design parameters. When the tolerance of d_{GO} and d_{TiO2} increases, the width of photonic band gap decreases. The error caused by the measurement results in the difference between the gap width and the theoretical calculation [32]. Since the experimentally prepared TiO_2 has poor crystallinity, and the refractive index in the simulation calculation is a near body structure, it will affect the disappearance of the photonic band gap [33].

3.6. Structure characterization of the samples

X-ray diffraction (XRD) was used to investigate the phase structure of the samples. Fig. 8 shows the XRD patterns of $(GO/TiO_2)_N$ one-dimensional photonic crystal, GO/TiO_2 composite film, and GO/TiO_2 powder. Among them, the peak at 11.1° of 2θ can be found, which corresponds to the (001) plane of GO [34]. The diffraction peak at 48.0°, 55.1°, and 68.8° of 2θ can be indexed to the (200), (211), and (116) planes of anatase TiO_2, respectively (JCPDS No. 21-1272). As for $(GO/TiO_2)_N$ one-dimensional photonic crystal, the peaks at 18.2°, 28.2°, 30.1°, and 49.4° correspond to (103), (211), (213), and (300) planes of carbon. While for GO/TiO_2 composite film and GO/TiO_2 powder, the peaks at 14.1°, 19.6°, 28.2°, 29.5°, and 60.0° correspond to (102), (112), (211), (203), and (106) planes of carbon. The results confirm that the obtained multilayered composite was GO/TiO_2 nanocomposite.

To understand the structure of photonic crystal multilay-

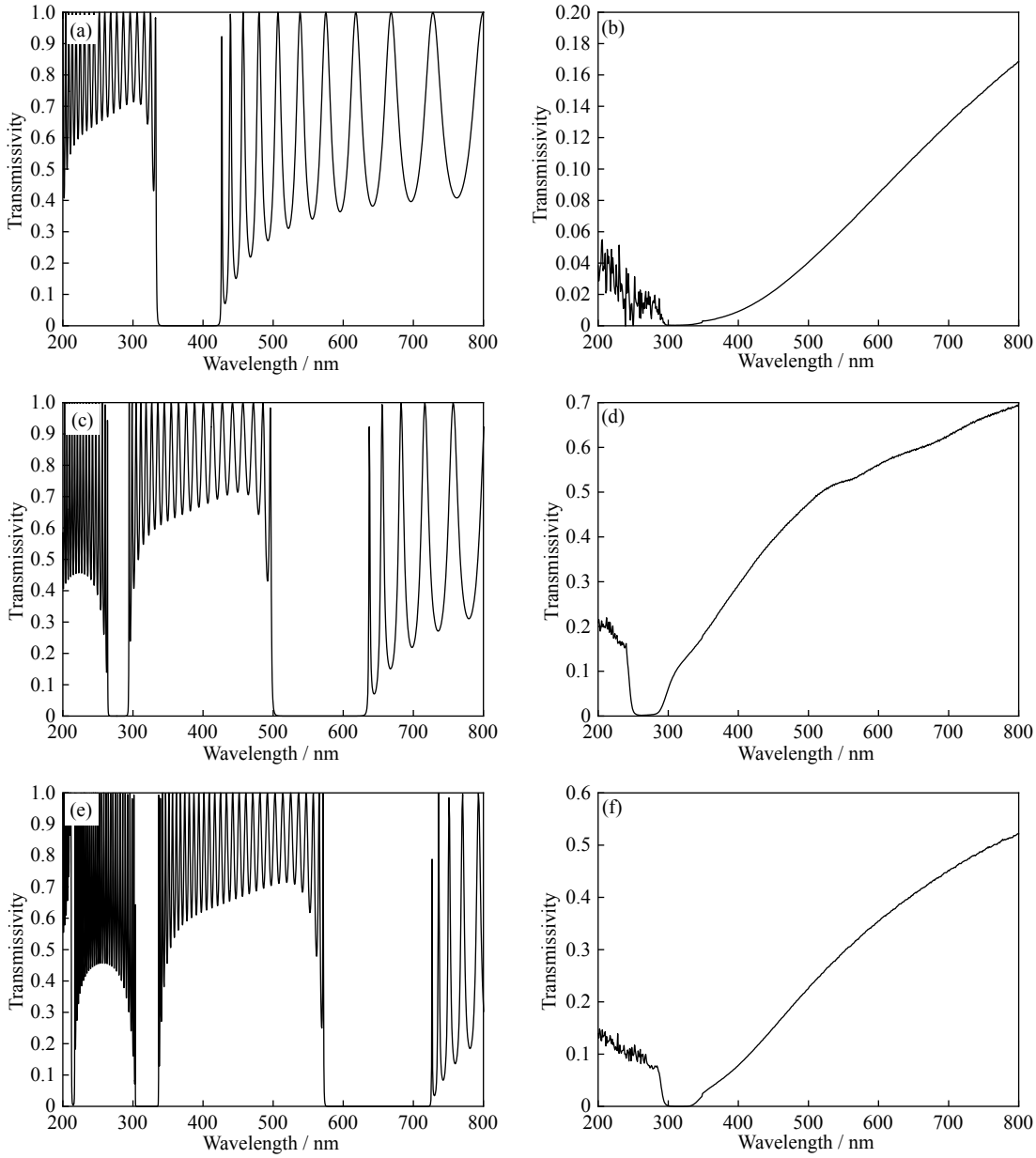

Fig. 7. Calculation and experimental transmission curves of $(GO/TiO_2)_N$ multilayer films with different lattice constants: (a) 73 nm, calculated transmission curve; (b) 73 nm, experimental transmission curve; (c) 109 nm, calculated transmission curve; (d) 109 nm, experimental transmission curve; (e) 125 nm, calculated transmission curve; (f) 125 nm, experimental transmission curve.

ers, we tried to take photos with an optical microscope. Twenty-one layers of $(GO/TiO_2)_N$ photonic crystals were prepared via layer-by-layer spin coating method. The special structure could not be clearly identified by scanning electron microscopy and transmission electron microscopy; therefore, we used a tape to create multilayer structure of the steps stating on the edge of the photonic crystals to indicate $(GO/TiO_2)_N$ photonic crystals. The layer-by-layer steps structure can be clearly seen in Fig. 9.

3.7. Photocatalytic activity

Fig. 10 shows the photocatalytic degradation curves of $(GO/TiO_2)_N$ one-dimensional photonic crystal, GO/TiO_2 composite film, and GO/TiO_2 powder. The photonic crystal shows lattice constant d = 125 nm, periodic layer number N = 21, filling ratio d_{GO}/d = 0.45, and incident angle of 0°. The photonic crystal and GO/TiO_2 powder show a better photocatalytic degradation performance than the composite film. The contact area between nano-powders and pollutants was larger than that of the composite film. The composite film only had one side in contact with the pollutants, while nano-powders were in full contact with the pollutants, which is conducive to photocatalytic performance [35]. The $(GO/TiO_2)_N$ one-dimensional photonic crystal exhibited a

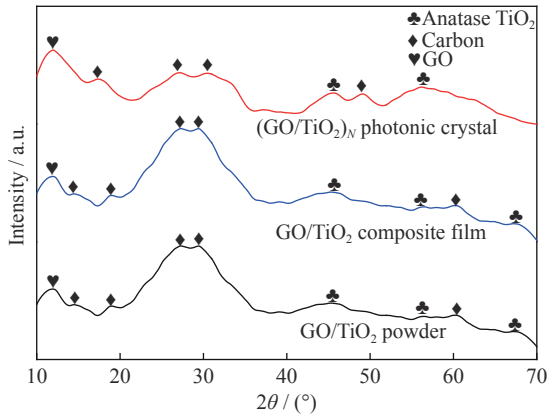

Fig. 8. XRD patterns of $(GO/TiO_2)_N$ one-dimensional photonic crystal, GO/TiO_2 composite film, and GO/TiO_2 powder.

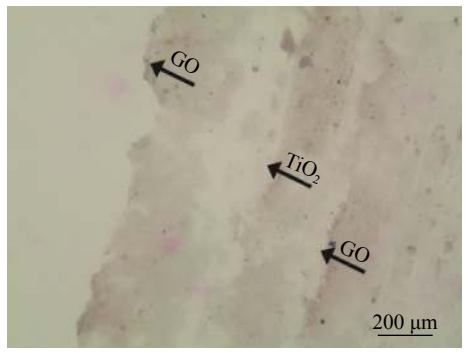

Fig. 9. Optical image of $(GO/TiO_2)_N$ one-dimensional photonic crystals.

better photocatalytic degradation efficiency of tetracycline in 60 min. The degradation efficiency of tetracycline by $(GO/TiO_2)_N$ one-dimensional photonic crystal reached 64%, was slightly lower than that by $(GO/TiO_2)_N$ one-dimensional photonic crystal. The degradation efficiency of tetracycline by GO/TiO_2 powder was 56% in 60 min, while the removal rate of tetracycline by GO/TiO_2 composite film was 25% in the same irradiation time. The photonic crystal featured a slow photonic effect region at 357 nm, which is close to the absorption band edge of tetracycline (357 nm), and greatly improved the photocatalytic efficiency. As shown in Fig. 10(b), according to the kinetic equation $-\ln(C/C_0) = kt$; here, t is the reaction time, k is the reaction rate constant, and the calculated rate constants were 0.01607, 0.01207, and 0.00438 min^{-1} for $(GO/TiO_2)_N$ one-dimensional photonic crystal, GO/TiO_2 powder, and GO/TiO_2 composite film, respectively.

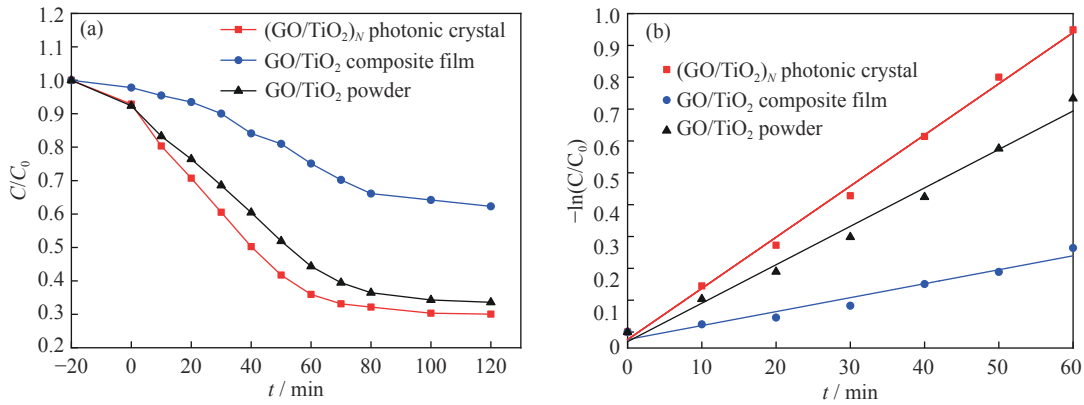

Fig. 10. Photocatalytic degradation curves (a) and kinetic curves (b) of $(GO/TiO_2)_N$ one-dimensional photonic crystal, GO/TiO_2 composites film, and GO/TiO_2 powder.

4. Conclusions

In this study, the multilayer structure of $(GO/TiO_2)_N$ one-dimensional photonic crystal was constructed by using the software of Translight, and the optical properties of $(GO/TiO_2)_N$ one-dimensional photonic crystal structure were calculated by using the transfer matrix method, and the influence of different parameters on the photonic band gap is analyzed. When the lattice constants increased from 73 to 150 nm, the central wavelength red-shifted and the gap width increased. When the filling ratio increased, the central wavelength blue-shifted and the gap width first increased and then decreased. When the number of periodic layers increased, the central wavelength of the band gap did not change; the gap width remained unchanged when the number of periodic layers increased to a certain extent. When the incident angle increased, the central wavelength blue-shifted and the gap width decreased. When $N = 21$, $d_{GO}/d = 0.45$, $\theta = 0°$, $d = 125$ nm, a band gap with a width of 38 nm existed at the central wavelength of 320 nm. A one-dimensional photonic crystal film with a lattice constant of 125 nm was prepared via the sol–gel method; it is with a band gap of 53 nm existed at the center wavelength of 322 nm. The experimental results agree with the calculated results, which indicates that the $(GO/TiO_2)_N$ one-dimensional photonic crystal was successfully fabricated. The $(GO/TiO_2)_N$ one-dimensional photonic crystal had a slow photon region at 357 nm, and it showed a higher photocatalytic activity than the GO/TiO_2

powder and GO/TiO_2 composite film. Within 60 min, the removal rate of tetracycline reached 64%.

Acknowledgements

Thanks to Professor Pei-de Han and Li-qing Qiao of Taiyuan University of Technology for their help during the discussion of this work, and Wen-bin Cao of University of Science and Technology Beijing for his assistance and guidance. This work was financially supported by the National Key R&D Program of China (No. 2016YFC0700904).

References

[1] X.B. Chen, L. Liu, P.Y. Yu, and S.S. Mao, Increasing solar absorption for photocatalysis with black hydrogenated titanium dioxide nanocrystals, *Science*, 331(2011), No. 6018, p. 746.

[2] R.Q. Gao, Q. Sun, Z. Fang, G.T. Li, M.Z. Jia, and X.M. Hou, Preparation of nano-TiO_2/diatomite-based porous ceramics and their photocatalytic kinetics for formaldehyde degradation, *Int. J. Miner. Metall. Mater.*, 25(2018), No. 1, p. 73.

[3] D.F. Zhang, X.P. Pu, K.P. Du, Y.M. Yu, J.J. Shim, P.Q. Cai, S.I. Kim, and H.J. Seo, Combustion synthesis of magnetic Ag/$NiFe_2O_4$ composites with enhanced visible-light photocatalytic properties, *Sep. Purif. Technol.*, 137(2014), p. 82.

[4] R. Kullaiah, L. Elias, and A.C. Hegde, Effect of TiO_2 nanoparticles on hydrogen evolution reaction activity of Ni coatings, *Int. J. Miner.Metall. Mater.*, 25(2018), No. 4, p. 472.

[5] S. Pal, A.R. Yadav, M.A. Lifson, J.E. Baker, P.M. Fauchet, and B.L. Miller, Selective virus detection in complex sample matrices with photonic crystal optical cavities, *Biosens. Bioelectron.*, 44(2013), p. 229.

[6] W. Vallejo, A. Rueda, C. Diaz-Uribe, C. Grande, and P. Quintana, Photocatalytic activity of graphene oxide–TiO_2 thin films sensitized by natural dyes extracted from Bactris guineensis, *Roy. Soc. Open Sci.* 6(2019), No. 3, art. No. 181824.

[7] H.P. Qi, H.L. Wang, D.Y. Zhao, and W.F. Jiang, Preparation and photocatalytic activity of Ag-modified GO–TiO_2 mesocrystals under visible light irradiation, *Appl. Surf. Sci.*, 480(2019), p. 105.

[8] G. Collins, E. Armstrong, D. McNulty, S. O'Hanlon, H. Geaney, and C. O'Dwyer, 2D and 3D photonic crystal materials for photocatalysis and electrochemical energy storage and conversion, *Sci. Technol. Adv. Mater.*, 17(2016), No. 1, p. 563.

[9] G.X. Li, A. Boltasseva, and S. Zouhdi, Feature issue introduction: Metamaterials, photonic crystals and plasmonics, *Opt. Mater. Express*, 9(2019), No. 5, p. 2400.

[10] E. Yablonovitch, Inhibited spontaneous emission in solid-state physics and electronics, *Phys. Rev. Lett.*, 58(1987), No. 20, p. 2059.

[11] S. John, Strong localization of photons in certain disordered dielectric superlattices, *Phys. Rev. Lett.*, 58(1987), No. 23, p. 2486.

[12] A.N. Bugay and V.A. Khalyapin, Analytic description of pulse frequency self-shift in nonlinear photonic crystal fibers, *Commun. Nonlinear Sci. Numer. Simul.*, 75(2019), p. 270.

[13] A.C. Arsenault, D.P. Puzzo, I. Manners, and G.A. Ozin, Photonic-crystal full-colour displays, *Nat. Photonics*, 1(2007), p. 468.

[14] D.G. Ouzounov, F.R.M. Ahmad, D. Müller, N. Venkataraman, M.T. Gallagher, M.G. Thomas, J. Silcox, K.W. Koch, and A.L. Gaeta, Generation of megawatt optical solitons in hollow-core photonic band-gap fibers, *Science*, 301(2003), No. 5640, p. 1702.

[15] A. Diamantopoulou, E. Sakellis, G.E. Romanos, S. Gardelis, N. Ioannidis, N. Boukos, P. Falaras, and V. Likodimos, Titania photonic crystal photocatalysts functionalized by graphene oxide nanocolloids, *Appl. Catal.*, 240(2019), p. 277.

[16] J. Liu, H. Zhao, M. Wu, B. Van der Schueren, Y. Li, O. Deparis, J.H. Ye, G.A. Ozin, T. Hasan, and B.L. Su, Slow photons for photocatalysis and photovoltaics, *Adv. Mater.*, 29(2017), No. 17, p. 1605349.

[17] P. Li, Y. Wang, S.L. Chen, and A.J. Wang, Enhancement of gas–solid photocatalytic activity of nanocrystalline TiO_2 by SiO_2 opal photonic crystal, *J. Mater. Sci.*, 51(2016), No. 4, p. 2079.

[18] X.D. Lu, S.X. Lun, T. Zhou, and M. Zhang, A low-cost high-efficiency crystalline silicon solar cell based on one-dimensional photonic crystal front surface textures, *J. Opt.*, 15(2013), No. 7, art. No. 075705.

[19] I. Chopra and M. Roberts, Tetracycline antibiotics: mode of action, applications, molecular biology, and epidemiology of bacterial resistance, *Microbiol. Mol. Biol. Rev.*, 65(2001), No. 2, p. 232.

[20] H. Chen, S. Chen, X. Quan, and Y.B. Zhang, Structuring a TiO_2-based photonic crystal photocatalyst with Schottky junction for efficient photocatalysis, *Environ. Sci. Technol.*, 44(2010), No. 1, p. 451.

[21] J.Y. Li, X.A. Dong, Y.J. Sun, W.L. Cen, and F. Dong, Facet-dependent interfacial charge separation and transfer in plasmonic photocatalysts, *Appl. Catal. B*, 226(2018), p. 269.

[22] H. Esmaili, A. Kotobi, S. Sheibani, and F. Rashchi, Photocatalytic degradation of methylene blue by nanostructured Fe/FeS powder under visible light, *Int. J. Miner. Metall. Mater.*, 25(2018), No. 2, p. 244.

[23] S.N. Li, R.X. Ma, and C.Y. Wang, Solid-phase synthesis of Cu_2MoS_4 nanoparticles for degradation of methyl blue under a halogen-tungsten lamp, *Int. J. Miner. Metall. Mater.*, 25(2018), No. 3, p. 310.

[24] P.M. Bell, J.B. Pendry, L.M. Moreno, and A.J. Ward, A program for calculating photonic band structures and transmission coefficients of complex structures, *Comput. Phys. Commun.*, 85(1995), No. 2, p. 306.

[25] Z. Zhang and S.S. Satpathy, Electromagnetic wave propagation in periodic structures: Bloch wave solution of Maxwell's equations, *Phys. Rev. Lett.*, 65(1990), No. 21, p. 2650.

[26] A.J. Ward and J.B. Pendry, Calculating photonic Green's functions using a nonorthogonal finite-difference time-domain method, *Phys. Rev. B*, 58(1998), No. 11, p. 7252.

[27] C. Yao, *Fabrication of Titania/Graphene Oxide One-Dimensional Photonic Crystals and Research of Theirs Applications* [Dissertation], Southeast University, Nanjing, 2015, p. 88.

[28] A.M. Ahmed and A. Mehaney, Ultra-high sensitive 1D porous silicon photonic crystal sensor based on the coupling of Tamm/Fano resonances in the mid-infrared region, *Sci. Rep.*, 9(2019), No. 1, art. No. 6973.

[29] Y.I. Wang, S. Liu, and S.Y.Zhong, Tunable multichannel terahertz filtering properties of dielectric defect layer in one-dimensional magnetized plasma photonic crystal, *Opt. Commun.*, 473(2020), art. No. 125985.

[30] Z. Li, Z. Ge, X.Y. Zhang, Z.Y. Hu, D. Zhao, and J.W. Wu, Analysis of photonic band gaps in metamaterial-based one-dimensional ternary photonic crystals, *Indian J. Phys.*, 93(2019),

No. 4, p. 511.
[31] M. Libman, N.M. Kondratyev, and M.L. Gorodetsky, Semi-analytical model for a slab one-dimensional photonic crystal, *AIP Conference Proceedings*, 1936(2018), No. 1, art. No. 020004.
[32] M.I. Wafa, Y.M. EI-Batawy, and S.A. EI-Naggar, Stochastic analysis for one dimensional photonic crystals, *Optik*, 208(2020), art. No. 164106.
[33] X. Zhang, *Study on the Optical Properties of TiO_2/Metal(Dioxide) Multilayer Films* [Dissertation], Taiyuan University of Technology, Taiyuan, 2012, p. 70.
[34] B.F. Mohazzab, B. Jaleh, M. Nasrollahzadeh, Z. Issaabadi, and R.S. Varma, Laser ablation-assisted synthesis of GO/TiO_2/Au nanocomposite: Applications in $K_3[Fe(CN)_6]$ and Nigrosin reduction, *Mol. Catal.*, 473(2019), art. No. 110401.
[35] W.W. Zhang, J.Y. Zhang, Z.Y. Chen, and T.M. Wang, Photocatalytic degradation of methylene blue by $ZnGa_2O_4$ thin films, *Catal. Commun.*, 10(2009), No. 13, p. 1781.